Human Brain Mapping

WILEY

RESEARCH ARTICLE OPEN ACCESS

Beyond Focal Lesions: Dynamical Network Effects of White Matter Hyperintensities

Riccardo Leone[1,2,3] | Steven Geysen[3,4] | Gustavo Deco[5,6] | Xenia Kobeleva[1,3,4] | Alzheimer's Disease Neuroimaging Initiative

[1]Computational Neurology Group, Ruhr University Bochum, Bochum, Germany | [2]Faculty of Medicine, University of Bonn, Bonn, Germany | [3]German Center for Neurodegenerative Diseases (DZNE), Bonn, Germany | [4]Department of Neurology, University Hospital Bonn, Bonn, Germany | [5]Department of Information and Communication Technologies, Center for Brain and Cognition, Computational Neuroscience Group, Universitat Pompeu Fabra, Barcelona, Spain | [6]Institució Catalana de la Recerca i Estudis Avançats (ICREA), Barcelona, Spain

Correspondence: Xenia Kobeleva (xkobeleva@gmail.com)

Received: 8 August 2024 | **Revised:** 3 November 2024 | **Accepted:** 11 November 2024

Funding: X.K. was supported by an add-on fellowship of the Joachim Herz Foundation, a grant of the Transdisciplinary Research Area 1 of the University of Bonn, the Innovative Minds Programme of the Stiftung Deutsche Demenzhilfe, and the BONFOR research group support by University Hospital of Bonn. G.D. was supported by the project NEurological MEchanismS of Injury, and Sleep-like cellular dynamics (NEMESIS) (ref. 101071900) funded by the EU ERC Synergy Horizon Europe; the NODYN Project PID2022-136216NB-I00 financed by the MCIN/AEI, UE, the Ministry of Science and Innovation, the State Research Agency and the European Regional Development Fund; the AGAUR research support grant (ref. 2021 SGR 00917) funded by the Department of Research and Universities of the Generalitat of Catalunya, and the project eBRAIN-Health—Actionable Multilevel Health Data (id 101058516), funded by the EU Horizon Europe.

Keywords: connectivity | dementia | disconnectome | fMRI | neural-mass modeling | white matter hyperintensities | whole-brain modeling

ABSTRACT

White matter (WM) tracts shape the brain's dynamical activity and their damage (e.g., white matter hyperintensities, WMH) yields relevant functional alterations, ultimately leading to cognitive symptoms. The mechanisms linking the structural damage caused by WMH to the arising alterations of brain dynamics is currently unknown. To estimate the impact of WMH on brain dynamics, we combine neural-mass whole-brain modeling with a virtual-lesioning (disconnectome) approach informed by empirical data. We account for the heterogeneous effects of WMH either on inter-regional communication (i.e., edges) or on dynamics (i.e., nodes) and create models of their local versus global, and edge versus nodal effects using a large fMRI dataset comprising 188 non-demented individuals (120 cognitively normal, 68 with mild cognitive impairment) with varying degrees of WMH. We show that, although WMH mainly determine local damage to specific WM tracts, these lesions yield relevant global dynamical effects by reducing the overall synchronization of the brain through a reduction of global coupling. Alterations of local nodal dynamics through disconnections are less relevant and present only at later stages of WMH damage. Exploratory analyses suggest that education might play a beneficial role in counteracting the reduction in global coupling associated with WMH. This study provides generative models linking the structural damage caused by WMH to alterations in brain dynamics. These models might be used to evaluate the detrimental effects of WMH on brain dynamics in a subject-specific manner. Furthermore, it validates the use of whole-brain modeling for hypothesis-testing of structure–function relationships in diseased states characterized by empirical disconnections.

1 | Introduction

The structural scaffold formed by white matter connections shapes cerebral dynamical activity (Sporns 2013; Suárez et al. 2020). Its damage results in disruption of the arising dynamics (Alstott et al. 2009; Cabral et al. 2012; Idesis et al. 2022; Thiebaut de Schotten, Foulon, and Nachev 2020), ultimately yielding cognitive deficits (Jenkins et al. 2021; Thiebaut de Schotten, Foulon, and Nachev 2020). White matter hyperintensities (WMH) constitute imaging correlates of white matter

This is an open access article under the terms of the Creative Commons Attribution-NonCommercial License, which permits use, distribution and reproduction in any medium, provided the original work is properly cited and is not used for commercial purposes.

© 2024 The Author(s). *Human Brain Mapping* published by Wiley Periodicals LLC.

Summary

- White matter hyperintensities (WMH) appear in imaging studies as damage to focal white matter tracts, but they induce dynamical effects on interregional communication at a global level.
- In later stages of white matter damage, WMH might also determine changes in intrinsic regional brain node dynamics through disconnections.
- Whole-brain modeling can be used to effectively link structural damage to associated alterations of brain dynamics.

damage and are characterized by local areas of high signal in T2-weighted MRI (Kantarovich et al. 2022; Wardlaw, Valdés Hernández, and Maniega 2015). They pathologically correspond to vasculopathy, chronic demyelination, axonal damage and loss (Wardlaw, Valdés Hernández, and Maniega 2015). Previous studies demonstrated that WMH is associated with alterations of brain dynamics with significant effects both on static functional connectivity (FC) and time-varying FC (tv-FC) (Jenkins et al. 2021; Kantarovich et al. 2022; Schlemm et al. 2022; Schulz et al. 2021). Nonetheless, these studies lacked a generative model allowing them to explain these modifications and to compare different pathophysiological hypotheses. Understanding the effects of WMH is of crucial clinical importance due to their high prevalence and associated risk of developing cognitive impairment (Debette and Markus 2010; Wardlaw, Valdés Hernández, and Maniega 2015). Better elucidation of the pathophysiological effects of WMH on brain dynamics might provide insights for the development of new preventive and treatment strategies aimed at counteracting their detrimental effects. Furthermore, generative models of brain signal alterations caused by WMH might prove useful to predict subject-specific network dynamics alterations stemming from WM lesions in a clinical setting.

By linking structural connectivity to the arising dynamics through well-defined mathematical equations, whole-brain neural mass models (WBM) are well suited to explore the dynamical effects of structural lesions, such as WMH (Alstott et al. 2009; Cabral et al. 2012; Deco et al. 2017; Idesis et al. 2022). In WBM, model parameters can be adjusted based on hypotheses about the pathophysiological effects of the investigated observables (e.g., lesions of white matter tracts) and the biological plausibility of these hypotheses can be tested in terms of goodness of fit between simulated and empirical fMRI or EEG data (Kobeleva et al. 2022). From a network perspective, by interrupting the communication between various brain regions, WMH can be conceptualized as disconnections (Griffis et al. 2021; Idesis et al. 2022; Thiebaut de Schotten, Foulon, and Nachev 2020). As shown by a previous computational study, disconnections unlink each regional activity from that of other network's nodes, thus affecting the resulting FC (Cabral et al. 2012). Although promising, previous theoretical studies evaluating the impact of disconnections lacked validation by empirical data analyses, thus limiting the clinical applicability of whole-brain mass models for diagnostic or prognostic purposes.

In this study, by combining WBM with a virtual-lesioning disconnectome approach—informed by empirical WMH lesions—we aim to contribute to a deeper understanding of the effect of structural alterations caused by WMH on resting-state brain dynamics, going beyond focal lesion studies such as in stroke (Idesis et al. 2022). We introduce the concept that WMH might result in changes in the intrinsic dynamics of disconnected regions and build upon previous theoretical results (Cabral et al. 2012) by testing theoretical predictions against empirical data. Specifically, we aim to: (a) test how WMH influence inter-regional connectivity (structural disconnectivity models) and neuronal activity at the node level (node disconnectivity models), and (b) determine whether WMH effects are localized (i.e., focal) or indicative of more diffuse white matter damage (i.e., global). To achieve this, we developed four distinct WMH-weighted models to explore these hypotheses and compared them to a baseline benchmark model with no information regarding WMH. Our modeling approach is based on resting-state fMRI data of 188 elderly nondemented study participants (either cognitively normal or with mild cognitive impairment), constituting one of the largest data-driven WBM studies to date.

2 | Materials and Methods

2.1 | Participants

From an initial sample of 363 elderly subjects without dementia from the Alzheimer's Disease NeuroImaging Initiative 3 dataset, 188 subjects with available rs-fMRI, 3D-T1-weighted and 3D-FLAIR sequences, acquired at 3T at the same timepoint, were included after preprocessing. CSF biomarkers, including the amyloid-beta peptide 42 to 40 ratio (Aβ42/Aβ40) and total tau levels, were obtained from the UPENNBIOMK Master data release (Shaw et al. 2009). The detailed step-by-step inclusion and exclusion flowchart is summarized in Figure S1. In exploratory analyses, we assessed the associations between model-derived parameters of the homogeneous SDC model (i.e., the model with the best fit) and executive functions and memory. We used the composite measurements of executive functions and memory provided in the ADNI database. The full details are in Gibbons et al. (2012).

2.2 | MRI Preprocessing and Timeseries Extraction

The full MRI acquisition and preprocessing protocol is provided in the Supporting Information. Briefly, fMRIPrep v. 21.0.4 (Esteban et al. 2019) was used for fMRI preprocessing. XCP-D (Adebimpe et al. 2023) was used to discard the first four timepoints, to perform the "nonaggressive" ICA-AROMA denoising strategy (including six motion estimates and their derivatives as well as signal from white matter and CSF), and to extract regional timeseries for the 90 supratentorial regions of the automated anatomical labeling (AAL) atlas (Tzourio-Mazoyer et al. 2002) (Figure 1A and Table S1). Timeseries were demeaned, detrended and filtered in the 0.04–0.07 Hz frequency range.

2.3 | Structural Connectivity

To avoid the possible detrimental effects of WMH on diffusion tractography (Min et al. 2021; Svärd et al. 2017), we used a

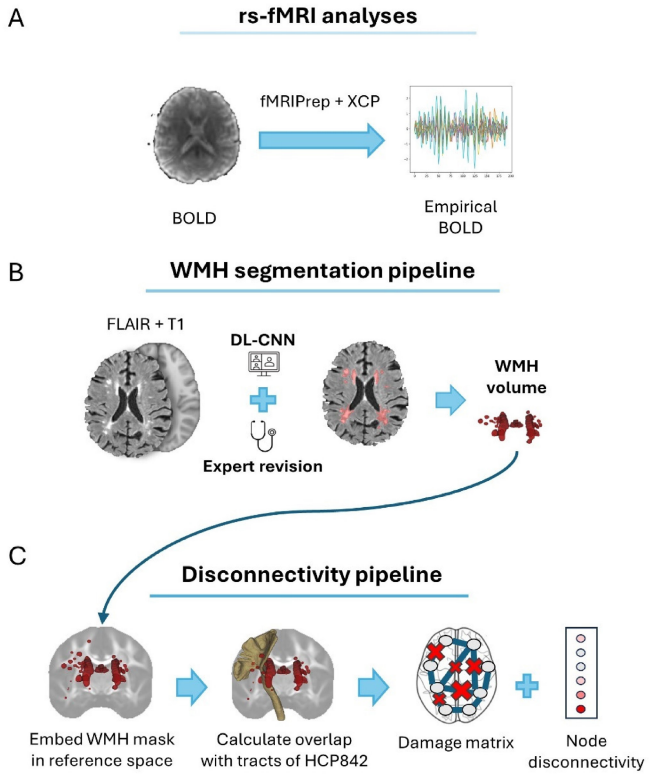

FIGURE 1 | Preprocessing workflow of the study. (A) fMRI data preprocessing was performed using the reproducible containerized versions of fMRIPrep (Esteban et al. 2019) and XCP (Adebimpe et al. 2023). (B) WMH segmentation was performed in subject space via automated deep learning software and visually checked to avoid inconsistencies. Infratentorial WMH were removed. (C) MNI-registered WMH masks were used as input for the Lesion Quantification Toolkit to calculate subject-specific damage matrices, representing the percentage of damage to each regional connection (represented by an "X" of different dimensions on the damaged tract) and a node disconnection vector, summarizing, for each brain region, the extent of regional disconnection from the whole-brain network (represented by different shades of red; gray defines nodes that were not disconnected by WMH).

normative SC matrix based on the AAL atlas from a previously published study in healthy controls (Škoch et al. 2022).

2.4 | WMH Segmentation and Disconnectome Analysis

Segmentation of WMHs was performed using a deep-learning-based software (Li et al. 2018) in subject space (Figure 1B). Segmentations were visually inspected to avoid inconsistencies and manually modified, if needed. Infratentorial WMH were removed. Fazekas score (Fazekas et al. 1987) was recorded. Total WMH volumes were calculated in mm^3, log-transformed and normalized to the 0–1 range (only in the group with relevant WMH, namely the volume for subjects without relevant WMH was set to 0). WMH segmentations were registered to MNI space and used as inputs for the Lesion Quantification Toolkit (LQT) (Griffis et al. 2021). The full details are reported in the original paper (Griffis et al. 2021) and graphically summarized in Figure 1C. Briefly, LQT employs a normative white matter atlas in MNI space to estimate the damage to each of 70 reference tracts caused by the input lesion. From this, a disconnection vector ($\vec{d}$) representing the WMH-related disconnection to each region and a damage matrix (DM) representing the percentage of damage to each edge are calculated.

2.5 | Hopf Model

We modelled each regional BOLD signal over time using the normal form of a supercritical Hopf bifurcation and coupled the resulting activity through the normative AAL atlas (Škoch et al. 2022; Figure 2A). The Hopf model has been widely used to describe whole-brain neural dynamics, given its ability to capture static and dynamic properties of brain functional connectivity (Deco et al. 2017). In the complex plane, the simulated BOLD activity (z) of each node (n) over time (t) is described by the following differential equation:

$$\frac{dz_n}{dt} = z\left[a_n + i\omega_n - \left|z_n^2\right|\right] + \beta\eta_n(t) \quad (1)$$

where z_n is a complex number $z_n = x_n + i\,y_n$, ω_n denotes the intrinsic frequency of each node, which is determined empirically by averaging the peak frequencies of narrowband-filtered BOLD signals in the 0.04–0.07 Hz range. We used group-averaged frequencies for all simulations. $\eta_n(t)$ represents additive Gaussian noise with standard deviation β. Substituting z_n in Equation (1) and dividing into the real and imaginary parts of the equation, we obtain:

$$\frac{dx_n}{dt} = \left[a_n - x_n^2 - y_n^2\right]x_n - \omega_n y_n + \beta\eta_n(t) \quad (2)$$

$$\frac{dy_n}{dt} = \left[a_n - x_n^2 - y_n^2\right]y_n - \omega_n x_n + \beta\eta_n(t) \quad (3)$$

Here, x_n represents the BOLD signal for a single uncoupled node. In the Hopf model, a_n, is known as the bifurcation parameter, and can be thought of as a control parameter governing the dynamical activity of each region. When the bifurcation parameter is negative ($a_n < 0$), the addition of Gaussian noise results in noisy activity around a stable point, which can be thought of as corresponding to asynchronous neuronal firing. After transitioning to values greater than the bifurcation point ($a = 0$), full oscillations are observed for positive values ($a_n > 0$), which correspond to synchronized neuronal firing.

Given that the brain is a coupled system consisting of various nodes (brain regions), the activity of all nodes is coupled through an underlying structural connectivity matrix C_{np}, which is defined as the number of streamlines connecting each two regions n and p. The real part of the complex number z_n representing the BOLD signal for node n when considering the coupled whole-brain system is then described by the following equation:

$$\frac{dx_n}{dt} = \left[a_n - x_n^2 - y_n^2\right]x_n - \omega_n y_n + G\sum_i C_{np}\left(x_p - x_n\right) + \beta\eta_n(t) \quad (4)$$

where G, defined as the global coupling weight, equally scales the total input received by each brain area to determine the overall synchronization. In the baseline model, we set the bifurcation parameter for all nodes at the brink of the bifurcation ($a_n = -0.02$),

as this nodal activity regime is able to give rise to complex collective brain dynamics resembling whole-brain activity observed in vivo (Deco, Jirsa, and McIntosh 2011; Deco et al. 2017). All simulations were implemented in Neurolib (Cakan, Jajcay, and Obermayer 2021). The sampling rate of 3 s and simulation length matched the empirical preprocessed fMRI recordings, plus two initial minutes—to allow for the stabilization of the system after the initial random conditions—that were discarded before other analyses.

2.6 | Model Fitting

As commonly performed in the literature (Deco et al. 2019; Patow et al. 2023), we initially aimed to best characterize both time-averaged and time-varying properties of the empirical data by calculating FC and tv-FC (Deco et al. 2019) in healthy subjects without WMH. In line with previous studies (Deco et al. 2019; Patow et al. 2023), fitting tv-FC was clearly a stronger model constraint compared with fitting FC in our dataset. As can be seen in Figure S2, FC fits are consistently high across a wide range of G (resulting in several possible G values to retrieve the same FC), while tv-FC clearly shows a global minimum at $G = 1.98$. This is an expected finding, as tv-FC is better able to capture the complex spatiotemporal structure inherent in fMRI data. Due to better constraints in model parameter estimation, we only focus on fitting tv-FC for further analyses.

Tv-FC was assessed using the phase functional connectivity dynamics (phFCD) (Deco et al. 2019). Briefly, for both empirical and

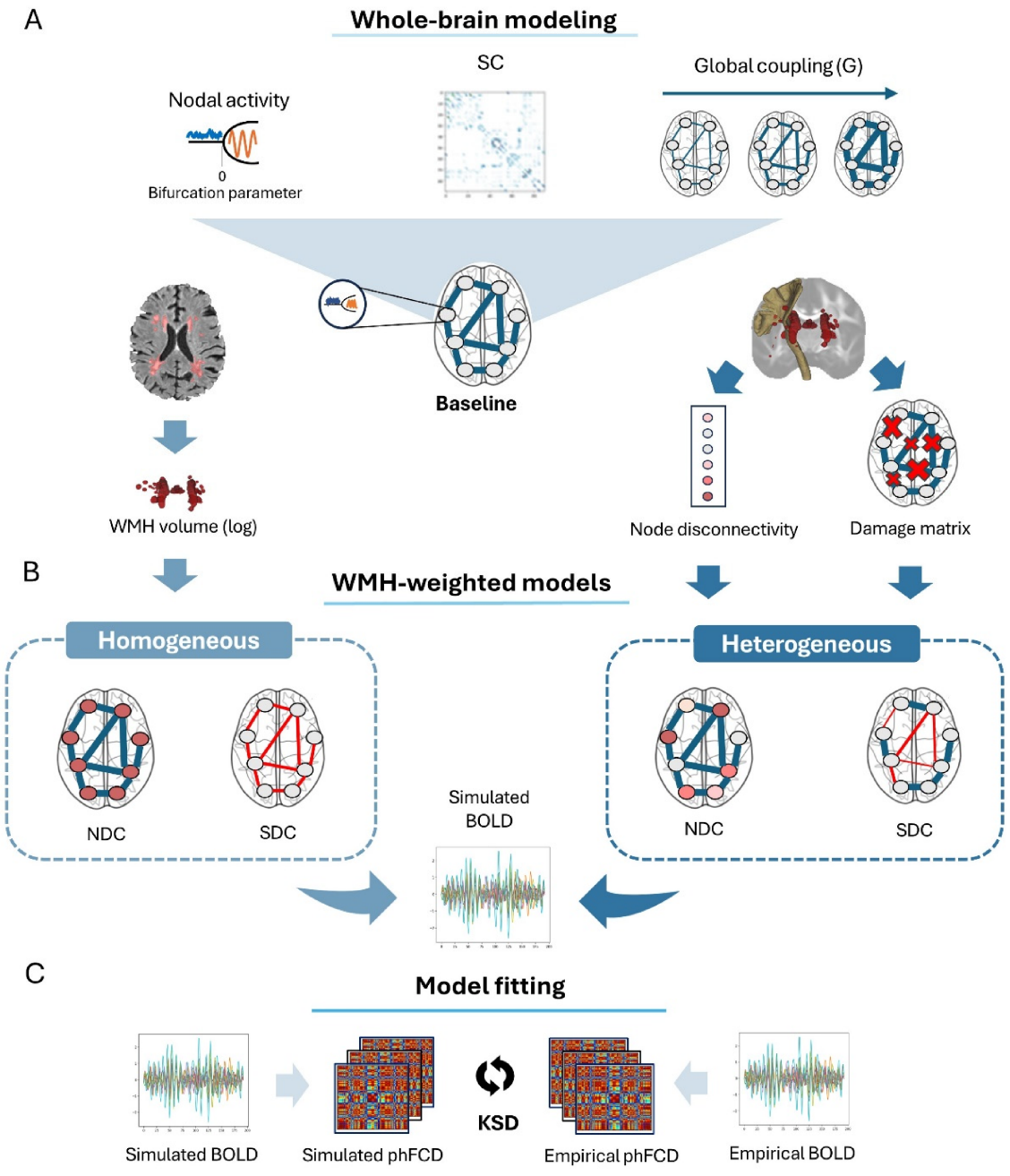

FIGURE 2 | Legend on next page.

simulated signals, we first applied the Hilbert transform to calculate the instantaneous BOLD phase of each region n at each timepoint t. For each timepoint, we then calculated its phase coherence matrix by taking the cosine of the absolute phase difference of each two regions n and m. When the BOLD signal in regions n and m is synchronized, it means that their phases would be similar, and, consequently, their phase difference is small, resulting in a high phase coherence value (close to 1). On the other hand, if their phases are not aligned (i.e., asynchronous), their phase coherence value is close to zero. Since the phase coherence matrix is symmetric, we only considered its upper triangular part and we accrued them over all timepoints for each subject or simulation. We finally compared the empirical and simulated distributions of the phFCD using the Kolmogorov–Smirnov distance (KSD). Lower KSD represents better goodness of fit (Figure 2C). The full details are in Deco et al. (2019).

2.7 | Modeling Steps

We hypothesized that WMH might have an impact on brain dynamics only after a certain threshold, so we used the clinical Fazekas score (Fazekas et al. 1987)—a visual estimate of the amount of WMH in structural MRI scans (score range 0–3)—to binarize our sample into a group without relevant WMH (Fazekas ≤ 1) and a group with relevant WMH (Fazekas >1). Previous studies using the Hopf model showed that brain dynamics in healthy subjects are best described by slightly subcritical bifurcation parameters (Deco et al. 2017). We assessed the optimal dynamical working point in our sample by performing a group-level tuning of the Hopf whole-brain model in the healthy subjects' group (no WMH and cognitively unimpaired). To do so, we fixed a (uniformly across regions) just below the critical bifurcation point ($a=-0.02$) and allowed G to vary as a free parameter (Figure 2B) ($0 \leq G \leq 3.5$, $\Delta G = 0.02$). The best G maximizing the fit to empirical data was found at 1.98. We refer to the resulting model (with $a=-0.02$ and $G=1.98$) as the baseline model and use it as a reference benchmark for comparison of all WMH-weighted models.

2.8 | WMH-Weighted Models

We first discuss the building blocks of WBM aimed at evaluating the effects of WMH on brain dynamics, tested in the subgroups with relevant WMH (88 subjects), and later presented the specific equations used for fitting. We developed four distinct WMH-weighted models (Figure 2B) guided by two sets of interrelated hypotheses: (Sporns 2013) how WMH might influence various parameters of the whole-brain model (i.e., edges vs. nodes), and (Suárez et al. 2020) the biological nature of WMH (i.e., local vs. global).

The first set of hypotheses explored how WMH might impact brain dynamics. Since WMH damage WM tracts, which are crucial for communication between brain regions, we posited that WMH could reduce the strength of inter-regional communication (i.e., the edges of the connectome), leading to structural disconnectivity (SDC) models. Additionally, experimental data suggest that axonal lesions could alter the intrinsic dynamic of neuronal firing (Nagendran et al. 2017). In the node disconnectivity (NDC) models, we tested whether these changes could be seen in the whole-brain Hopf models as variations in (nodal) bifurcation parameters. Based on previous studies (Demirtaş et al. 2017; Sanz Perl et al. 2023), we hypothesized that higher WMH-related disconnections might induce reductions in bifurcation parameters.

The second set of hypotheses addressed whether WMH effects are location-specific (i.e., local) or suggestive of a more diffuse WM damage (i.e., global). Biological evidence posits that WMH might represent just the observable aspect of a more widespread WM damage that is not visible with conventional MRI (Maillard et al. 2011; ter Telgte et al. 2018). We explored this concept by developing homogeneous models, which hypothesized that WMH effects are global and confronted them with heterogeneous models where the effects of WMH are locally confined to the specific brain regions or connections damaged by visible WMH.

To build the heterogeneous models, we used outputs from the LQT pipeline. For the heterogeneous SDC model, we linearly

FIGURE 2 | Schematics of the modeling pipeline. (A) In a whole-brain Hopf model, each regional dynamics over time is driven by its intrinsic frequency (not shown, as this was estimated from the empirical data and not modified in relation to WMH) and by a bifurcation parameter, describing the transition from asynchronous noisy behavior (<0) to full oscillations (>0), with zero referred to as the critical bifurcation point. The overall activity of the network is derived from the sum of the local activity plus the weighted (by the strength of inter-regional connection, e.g., number of tracts) sum of the activities of all regions connected to it, scaled by a global coupling parameter (G). Using this framework, a baseline model was constructed based on a normative SC and tuned to the empirical data of subjects without cognitive impairment and without WMH (Baseline model). (B) This panel displays the four WMH-weighted whole-brain models, categorized into homogeneous and heterogeneous types according to the hypotheses outlined in the main text. These models investigate whether WMH effects are localized to specific brain regions (heterogeneous) or distributed broadly across the brain (homogeneous). For the homogeneous models, the log-transformed volume of WMH is applied to uniformly reduce either connectivity or bifurcation parameters uniformly across the brain. In the homogeneous Node Disconnectivity (NDC) model, the bifurcation parameters in all regions are uniformly decreased, represented by red nodes with the same shade. In the homogeneous structural disconnectivity (SDC) model, connectivity across all tracts is uniformly reduced, shown as uniformly thinner red lines. In the heterogeneous models, the NDC model links WMH to changes in bifurcation parameters, using the node disconnectivity vector to inform how these parameters are altered in specific regions, depicted as red nodes of varying shades. Meanwhile, the SDC version simulates how WMH reduce inter-regional communication along specific tracts. This is achieved by using the damage matrix from the Lesion Quantification Toolkit to decrease connectivity only in those specific tracts, illustrated with red lines of varying thickness. The brain network illustration also includes gray nodes, which represent regions where WMH do not impact bifurcation parameters (matching the baseline model), and blue tracts, indicating connections not affected by WMH. These models were employed to simulate whole-brain BOLD activity and were subsequently compared against empirical data and a baseline model without WMH information. (C) The dynamics of phase coherence matrices (phFCD) was chosen as the fitting measurement between simulated and empirical data and compared with the Kolmogorov–Smirnov distance (KSD, see Methods for a full description). Lower values of KSD represent a better fit.

reduced the edge values of the normative SC matrix by the subject-specific damage matrix. For the heterogeneous NDC model, we reduced the bifurcation parameters proportionally to the node disconnectivity vector. For the homogeneous models, we used the log-transformed WMH volume as a proxy of overall brain damage. The homogeneous SDC model was created by proportionally reducing the global coupling parameter, while the homogeneous NDC model involved proportionally decreasing all bifurcation parameters with increasing WMH volume.

To introduce information regarding WMH in the Hopf model we performed a linear fitting of one of its parameters (a, G, or SC) by WMH information (WMH volume log-transformed, node disconnectivity or damage matrix) and explored the parameter space using a grid search. More in detail, the NDC and SDC homogeneous models were obtained by fitting a or G, respectively, as follows:

$$a = -0.02 + w * \mathrm{WMH}_{\mathrm{vol}} + b\ (-0.1 \le \mathrm{w} \le 0,\ -0.05 \le \mathrm{b} \le 0,\ \Delta\mathrm{w} = \Delta\mathrm{b} = 0.005);$$

$$G = 1.98 + w * \mathrm{WMH}_{\mathrm{vol}} + b\ (-1 \le \mathrm{w} \le 0,\ \Delta\mathrm{w} = 0.1;\ -0.5 \le \mathrm{b} \le 0,\ \Delta\mathrm{b} = 0.05);$$

The heterogeneous SDC model was obtained by linearly reducing the weights of the SC based on the damage matrix calculated by LQT, as follows:

$$\mathrm{SC}_{\mathrm{het}} = \mathrm{SC} + w * \mathrm{DM}\ (-0.25 \le w \le 0,\ \mathrm{b} = 0,\ \Delta\mathrm{w} = 0.005)$$

Elements with values less than zero in the resulting matrix were reset to zero. This matrix was used instead than the healthy normative SC. The fitting of b was omitted considering that the average value of SC elements is approximately zero.

Finally, the heterogeneous NDC model used the region disconnection vector $\vec{d}$ as a spatial prior for linear fitting, leading to heterogeneous bifurcation parameters (different between regions):

$$\vec{a} = -0.02 + w * \vec{d} + b\ (-0.1 \le \mathrm{w} \le 0,\ -0.05 \le b \le 0,\quad \Delta w = \Delta b = 0.005).$$

Homogeneous random models were obtained by randomly shuffling WMH volume across subjects. The heterogeneous random versions were obtained by randomly shuffling the region disconnection vector or damage matrix between subjects for node and structural disconnectivity models, respectively.

2.9 | Statistical Comparisons

Categorical variables are reported as numbers (percentages) and continuous variables as median (interquartile ranges) and compared with the Chi-square and Mann–Whitney-U test, respectively. Models' goodness of fit was compared with the paired-samples Wilcoxon test and corrected for multiple comparisons with the Benjamini–Hochberg method (Benjamini and Hochberg 1995). Partial correlation analyses were performed using Spearman's correlation and corrected for age.

3 | Results

3.1 | Empirical Data Analysis

We first present the overall characteristics of the sample (Table S2 and Figure S3). We hypothesized that WMH might not have an impact on brain dynamics in the lowest Fazekas score group due to their very limited extension, thus we binarized our sample into a group without relevant WMH (Fazekas ≤ 1, 100 subjects) and a group with relevant WMH (Fazekas > 1, 88 subjects). We also later explored the effects of WMH on brain dynamics in the subgroup with the highest Fazekas score of 3 ("High WMH", 22 subjects). As expected, subjects with relevant WMH were significantly older than those without ($p < 0.001$). There were no statistically significant differences in years of education and mini-mental state examination (MMSE) between the two groups. WMH did not show any significant correlation with Aβ42/Aβ40 nor tau CSF levels (all $p > 0.05$; Figure S4). Figure 3A shows the regional distribution of WMH (Figure 3A); compared to the group without WMH, the group-averaged distribution of the phFCD was shifted towards lower values in individuals with WMH ($p < 0.001$), suggesting lower synchrony (Figure 3B).

3.2 | Model Comparison

Accounting for WMH-related damage resulted in better descriptions (lower KSD) of the empirical data compared to the baseline model (Figure 3C, for individual p values, please see Table 1). We found that WMH significantly alter inter-regional communication strengths (i.e., edges), although this effect remained statistically significant after correcting for multiple comparisons only for the homogeneous SDC model. We compared these models fits to the respective randomly implemented counterparts and found that random models resulted in significantly lower model fits for both SDC models (Figure S5, Table S3). Interestingly, both heterogeneous models did not result in increased model fit compared to their homogeneous counterparts. The volume of WMH (log-transformed) was significantly positively correlated with the percent improvement of model fit compared with baseline for all WMH-weighted models (Figure 3D). These analyses were performed considering partial correlation corrected for the effects of age (Table 2). Based on these findings, we assessed the dynamical effects of WMH in the group with the highest WMH (Fazekas score of 3). Here, the heterogeneous SDC and both NDC models described the empirical data significantly better compared to the baseline, also after multiple comparisons correction (Figure 3E), suggesting that at higher level of tract damage, an effect on regional node dynamics is also observed (Table 2).

3.3 | Assessing the Impact of Clinical Variables on Model Fit

We then performed exploratory correlational analyses (partial correlations, including the effects of age) to further evaluate if other clinical variables might be responsible for the increase in model fit compared to the baseline (Figure 4, Table 2). We

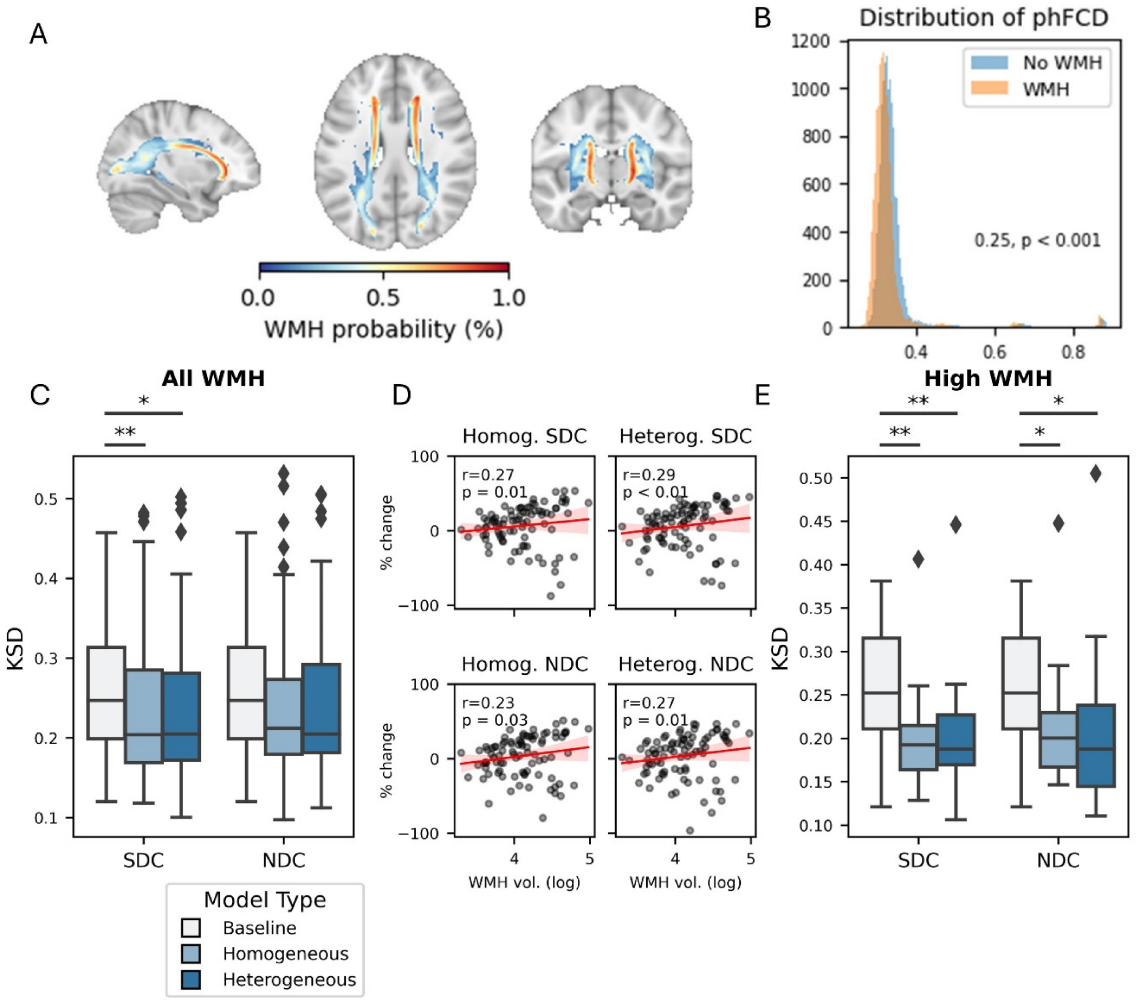

FIGURE 3 | (A) Maximum intensity projections along the sagittal (left), axial (middle) and coronal (right) planes of WMH probability maps. (B) Histograms of the distribution of the group-averaged phase functional connectivity dynamics (phFCD) in the groups without (blue) and with (orange) relevant WMH. The distribution of the phFCD is significantly shifted towards lower phFCD values in the group with relevant WMH, suggesting lower synchrony ($p < 0.001$). (C) Boxplots summarizing model comparisons between the baseline (white) and the homogeneous (light blue) and heterogeneous models (dark blue). The same baseline model (in white) is shown twice for better visualization of the comparison. Structural disconnectivity models (SDC), assessing the impact of WMH on structural connections are grouped on the left. Node disconnectivity (NDC) models, showing the effects of WMH on bifurcation parameters are shown as grouped boxplots on the right. The boxplots represent the Kolmogorov–Smirnov distance (KSD) between the empirical and simulated phase functional connectivity dynamics for the whole group with WMH. Note that after Benjamini–Hochberg correction only the homogeneous SDC remained statistically significant. (D) Scatterplots depicting the correlation between WMH volume (log-transformed, along the x axes) and the percentage of improvement in the model fit of the considered model (homogenous/heterogeneous SDC/NDC) compared to the baseline model (r refers to post hoc Spearman's rank-order partial correlation corrected for age, $p = p$-value). (E) The same model comparison as in (C) was evaluated in the group with the highest Fazekas score of 3. All comparisons remained statistically significant also after Benjamini–Hochberg correction. *$0.01 < p < 0.05$; **$0.001 < p <= 0.01$.

found that for both SDC models, the increase in performance was negatively correlated with years of patient education. For the heterogeneous SDC model, the observed improvement was also positively correlated with increasing age. No correlations were found between these variables and either of the NDC models (Figure S5, Table 2).

3.4 | Assessing the Association Between Model Parameters and Cognitive Scores

We performed exploratory analyses to investigate the association of model-derived parameters on cognitive scores of executive functions and memory. We focused on the homogeneous SDC model since this was the best-performing model. We did not find any statistically significant association between executive functions and memory scores (Figure S6).

4 | Discussion

In this study, we aimed to quantify in vivo global dynamical effects induced by WMH, which are highly prevalent lesions of the WM in the general aging population (Garnier-Crussard et al. 2023; Wardlaw, Valdés Hernández, and Maniega 2015). We combined WBM (Alstott et al. 2009; Cabral et al. 2012;

Deco et al. 2017; Demirtaş et al. 2017; Idesis et al. 2022; Patow et al. 2023; Sanz Perl et al. 2023) with a virtual-lesioning approach (Griffis et al. 2021) and tested different hypothesis-driven generative models of brain dynamics against empirical resting-state fMRI data, providing new insights into the pathophysiology of WMH from a network perspective. We tested various hypotheses on the local versus global and nodal versus edge effects of WMH in different WMH-weighted models and compared them both to a baseline model, to evaluate their added accuracy in describing empirical data, and to random models, to assess their robustness. We found that, although WMH are focal lesions of WM tracts, they induce global effects on network dynamics by reducing the global coupling of the network. At later stages of damage (e.g., higher WMH volume), WMH also alter the intrinsic nodal dynamics of disconnected regions. Finally, exploratory analyses suggested that level of education plays a role in counteracting the detrimental effects of WMH on global coupling, consistent with previous work on cognitive reserve (Stern 2009). Our results contribute to building biologically plausible and clinically informative models of brain dynamics in the healthy aging population and in diseases characterized by an elevated volume of WMH, such as cerebrovascular and Alzheimer's dementia (Garnier-Crussard et al. 2023; Wardlaw, Valdés Hernández, and Maniega 2015). Furthermore, methods and insights from this study might also be applied to other neurological diseases characterized by WM disconnections, that is, multiple sclerosis or traumatic brain injury.

TABLE 1 | Median (interquartile range) Kolmogorov–Smirnov distance (KSD) of the simulated phase functional connectivity dynamics compared to the empirical data for the baseline and WMH-weighted models.

	All WMH		High WMH	
Model Name	**KSD**	***p***	**KSD**	***p***
Baseline	0.25 (0.20–0.31)	NA	0.25 (0.21–0.31)	NA
Homogeneous SDC	0.20 (0.17–0.29)	**0.003***	0.19 (0.16–0.21)	**0.003***
Heterogeneous SDC	0.20 (0.17–0.28)	**0.042**	0.19 (0.17–0.23)	**0.005***
Homogeneous NDC	0.21 (0.18–0.27)	0.17	0.20 (0.16–0.22)	**0.036***
Heterogeneous NDC	0.21 (0.18–0.29)	0.12	0.19 (0.14–0.24)	**0.036***

Note: Results are first presented in the complete group consisting of all subjects with relevant WMH (All WMH) and then only for the group with a Fazekas score of 3 (High WMH). *p* values represent the comparison of model fit of each WMH-weighted model compared to the baseline model. Significant *p* values are illustrated in bold, and significant *p* values after multiple-comparison correction using the Benjamini–Hochberg correction are illustrated with *.
Abbreviations: NDC = node disconnectivity; SDC = structural disconnectivity.

We found that, when considering all subjects with WMH, SDC models yielded a significantly better fit compared to the baseline model, while NDC models performed better only when considering the specific subgroup with the highest Fazekas score (i.e., high WMH group). This finding suggests that alterations in inter-regional communication induced by WMH (as evidenced by SDC models) play a more prominent role in shaping global brain dynamics, namely reducing the strength of inter-regional communication (i.e., on the connectome edges). Only when a certain level of damage is reached, then disturbances in local nodal activity might play a role. In light of the location of WMH this is not an unexpected finding, but notably, modeling these effects considering the location-specific damage to WM tracts did not yield better descriptions of empirical data compared to considering their effect as globally homogeneous. This suggests that the damage associated with WMH might have dynamic repercussions at the whole-brain level. A previous study by Cabral et al. (2012) already showed in theoretical simulations that increasing levels of disconnections led to similar network reorganizations as reductions in global coupling. In this scenario, the more damage to white matter tracts, namely the higher the WMH load, the more the dynamical effects caused by disconnections resemble those occurring from a reduction in global coupling. From a biological perspective, a previous study also showed the existence of a widespread damage to white matter tracts that are not observable with structural MRI, of which WMH are just the tip-of-the-iceberg (Maillard et al. 2011; ter Telgte et al. 2018). WMH are surrounded by an area without abnormalities on conventional MRI, but where diffusion metrics in diffusion tractography are already altered (Maillard et al. 2011; Maniega et al. 2015). We suggest that these unobservable lesions might already determine communication impairments in widespread networks. In this scenario, the damage that was accounted for in the heterogeneous SDC model might thus be underestimated compared to the damage to the real empirical network. Thus, a global measure

TABLE 2 | Correlations (Spearman's *r*) between the percentage increase in model performance compared to the baseline for each WMH-weighted model and the considered demographic variables.

	Homogeneous SDC		Heterogeneous SDC		Homogeneous NDC		Heterogeneous NDC	
Demographic variable	***r***	***p***	***r***	***p***	***r***	***p***	***r***	***p***
WMH volume (log)	0.27	**0.01**	0.29	**0.007**	0.23	**0.03**	0.27	**0.01**
Age	0.15	0.16	0.23	**0.03**	0.21	0.052	0.10	0.35
MMSE	−0.19	0.08	−0.15	0.17	−0.13	0.23	−0.10	0.36
Education (years)	−0.26	**0.02**	−0.21	**0.045**	−0.21	0.055	0.16	0.14

Note: All correlations refer to partial correlations corrected for age, except for age itself. Significant *p* values are illustrated in bold.
Abbreviations: MMSE = Mini Mental State Examination; NDC = node disconnectivity; SDC = structural disconnectivity.

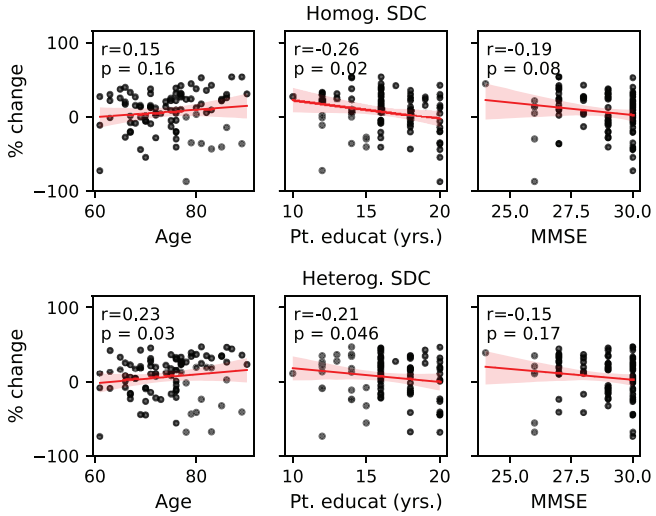

FIGURE 4 | Scatterplots depicting the correlation between demographics factors (age, years of patient education and mini-mental status examination (MMSE), and the percentage improvement in model performance of the considered model compared to the baseline model. The first row shows the results for the homogeneous structural disconnectivity model (SDC), while the second row shows the results for the heterogeneous SDC. For age, r refers to Spearman's rank correlation, while for patient education and MMSE, r refers to Spearman's partial correlation accounting for age. p = p-value, not corrected for multiple comparisons.

of WMH (since we perform a linear fitting) might be enough to capture this damage. Future studies using advanced diffusion-tractography-based measurements (e.g., fractional anisotropy) could further evaluate this hypothesis by also accounting for the normal-appearing white matter damage. Albeit previous associational studies on the effects of WMH on inter-regional FC are mixed (Schulz et al. 2021) and the association might be confounded by several factors (see next paragraph), our results are in line with the prevailing idea that WMH mostly reduces long-distance FC (Quandt et al. 2020; Yang et al. 2023) and consequently increase local efficiency (Vergoossen et al. 2021). The increase in local efficiency is also predicted by computational models characterized by a reduction in global coupling (Cabral et al. 2012), thus we are planning a future study to investigate whether this relationship can also be observed in our models fitted to empirical data of subjects with WMH.

Interestingly, for both SDC models, we found an inverse association between model performance increase—compared with the baseline—and years of education. We speculate that this finding might be related to nonlinearities occurring in vivo caused by counteracting increases in global coupling associated with higher educational status that could be linked to the construct of "cognitive reserve". Cognitive reserve refers to a series of protective mechanisms that allow an individual to mitigate the detrimental effects of age or pathological biomarkers (e.g., amyloid, tau, WMH) to achieve better results than what would have been predicted by simply evaluating the observed damage (Stern 2009). Previous studies demonstrated that cognitive reserve is indeed related to increases in resting-state functional connectivity in distributed resting-state networks (Marques et al. 2016), as well as with a more integrated and interconnected network configuration (Chaddock-Heyman et al. 2018). Given the exploratory nature of this finding, future studies are needed to further explore this hypothesis.

When WMH become widely diffuse throughout the brain, namely when the Fazekas score is 3, then a more negative shift away from the bifurcation parameter of the nodes is also observed, that is, the dynamical behavior of the networks becomes noisier. This reduction in bifurcation parameters might be linked to other known pathological processes also associated with WMH, especially at later stages, such as tau and amyloid (Demirtaş et al. 2017; Patow et al. 2023). However, our study did not find any significant correlation between WMH and CSF levels of Aβ42/Aβ40 nor tau, suggesting that, if present, the interplay among these pathologies might be more intricate and not simply linear in nature. An alternative hypothesis is that neurons might not suffer from alterations to their intrinsic patterns of firing when demyelination and axonal damage are below a certain threshold, possibly due to compensatory mechanisms (Naud and Longtin 2019). Only when this threshold is surpassed, then abnormal neuronal firing might occur. Future studies might implement biophysically detailed models and account for both WMH and amyloid/tau to try to disentangle their separate and synergistic contributions to intrinsic regional dynamics.

Some limitations apply to this study, some intrinsically linked to the methodology of rs-fMRI. The BOLD signal does not directly measure neuronal activity per se, but rather slow oscillations deriving from neuro-vascular coupling (Logothetis 2003; Logothetis and Wandell 2004). WMH are commonly associated with cerebral small vessel disease, thus, they might be associated with whole-brain level alterations of neuro-vascular coupling (Girouard and Iadecola 2006), increasing the intricacy in the interpretation of our results. Another limitation of our study is the age difference between the group with and without WMH. WMH are intrinsically associated with the aging process, resulting in an older average age for the cohort with WMH compared to the control group without WMH. To address the influence of the age difference, we evaluated the partial correlations corrected by age between increases in model performance and WMH and demographics variables. Furthermore, we used a normative SC for both groups, mitigating the potential impact of the age difference on SC measures. Another limitation is that model-derived parameters did not correlate with cognitive function scores, which are known to be impacted in subjects with WMH. A possible explanation is that in our study, we focused on fitting models to achieve the best average of single-subject fitting (i.e., using the same weight and bias for all subjects). While this resulted in models that could be applied to unseen subjects for a good representation of their dynamics, certain individual characteristics were not represented, leading to a lack of correlation with cognitive scores on a subject-specific basis. Lastly, our modeling approach, as common to many previous modeling studies using the Hopf model with rs-fMRI (Deco et al. 2017; Demirtaş et al. 2017; Sanz Perl et al. 2023), did not include delays due to the longer timescales of the BOLD signal acquisition (seconds vs. the millisecond scale of inter-neuronal signaling), but studying the heterogeneous effects of WMH on delays could be an interesting direction to explore in future studies.

In summary, our study provides further understanding of the dynamical effects of WMH, suggesting the presence of an

associated widespread damage to WM tracts with relevant dynamical effects on global synchronization and, at later stages, also on regional brain dynamics. The models developed in this study also show promise for clinical applications, that is, in predicting subject-specific network effects in the presence of WMH. The pathophysiological insights developed and discussed in this study might be used, alone or in combination with other biomarkers (e.g., tau and amyloid), to inform and create more biologically plausible representations of brain dynamics in several diseases characterized by WMH, such as Alzheimer's disease, but also in other pathologies harboring WM disconnections (e.g., multiple sclerosis, traumatic brain injury). Furthermore, our study highlights the importance of whole-brain modeling to reconcile theoretical predictions with the nuances and complexities arising from biological findings, effectively bridging the gap between the two.

Author Contributions

R.L.: conceptualization, formal analysis, writing – original draft, writing – review and editing. **S.G.:** data curation, writing – review and editing. **G.D.:** conceptualization, writing – review and editing. **X.K.:** conceptualization, formal analysis, writing – review and editing.

Acknowledgments

Data collection and sharing for this project was funded by the Alzheimer's Disease Neuroimaging Initiative (ADNI) (National Institutes of Health Grant U01 AG024904) and DOD ADNI (Department of Defense award number W81XWH-12-2-0012). ADNI is funded by the National Institute on Aging, the National Institute of Biomedical Imaging and Bioengineering, and through generous contributions from the following: AbbVie, Alzheimer's Association; Alzheimer's Drug Discovery Foundation; Araclon Biotech; BioClinica Inc.; Biogen; Bristol-Myers Squibb Company; CereSpir Inc.; Cogstate; Eisai Inc.; Elan Pharmaceuticals Inc.; Eli Lilly and Company; EuroImmun; F. Hoffmann-La Roche Ltd. and its affiliated company Genentech Inc.; Fujirebio; GE Healthcare; IXICO Ltd.; Janssen Alzheimer Immunotherapy Research & Development LLC.; Johnson & Johnson Pharmaceutical Research & Development LLC.; Lumosity; Lundbeck; Merck & Co. Inc.; Meso Scale Diagnostics LLC.; NeuroRx Research; Neurotrack Technologies; Novartis Pharmaceuticals Corporation; Pfizer Inc.; Piramal Imaging; Servier; Takeda Pharmaceutical Company; and Transition Therapeutics. The Canadian Institutes of Health Research is providing funds to support ADNI clinical sites in Canada. Private sector contributions are facilitated by the Foundation for the National Institutes of Health (www.fnih.org). The grantee organization is the Northern California Institute for Research and Education, and the study is coordinated by the Alzheimer's Therapeutic Research Institute at the University of Southern California. ADNI data are disseminated by the Laboratory for Neuro Imaging at the University of Southern California.

Consent

Patient informed consent was acquired by ADNI Investigators at each participating site.

Conflicts of Interest

The authors declare no conflicts of interest.

Data Availability Statement

The data set is owned by a third-party organization; the Alzheimer's Disease Neuroimaging Initiative (ADNI). Data are publicly and freely available from the http://adni.loni.usc.edu/data-samples/access-data/InstitutionalDataAccess/EthicsCommittee (contact via http://adni.loni.usc.edu/data-samples/access-data/) upon sending a request that includes the proposed analysis and the name of the lead investigator. Code to reproduce the analyses will be made available on https://github.com/computational-neurology upon publication of the results.

References

Adebimpe, A., M. Bertolero, K. Mehta, et al. 2023. XCP-D: A Robust Postprocessing Pipeline of fMRI Data. https://doi.org/10.5281/zenodo.7641626.

Alstott, J., M. Breakspear, P. Hagmann, L. Cammoun, and O. Sporns. 2009. "Modeling the Impact of Lesions in the Human Brain." *PLoS Computational Biology* 5: e1000408.

Benjamini, Y., and Y. Hochberg. 1995. "Controlling the False Discovery Rate: A Practical and Powerful Approach to Multiple Testing." *Journal of the Royal Statistical Society: Series B: Methodological* 57: 289–300.

Cabral, J., E. Hugues, M. L. Kringelbach, and G. Deco. 2012. "Modeling the Outcome of Structural Disconnection on Resting-State Functional Connectivity." *NeuroImage* 62: 1342–1353.

Cakan, C., N. Jajcay, and K. Obermayer. 2021. "Neurolib: A Simulation Framework for Whole-Brain Neural Mass Modeling." *Cognitive Computation* 15: 1132–1152. https://doi.org/10.1007/s12559-021-09931-9.

Chaddock-Heyman, L., T. B. Weng, C. Kienzler, et al. 2018. "Scholastic Performance and Functional Connectivity of Brain Networks in Children." *PLoS One* 13: e0190073.

Debette, S., and H. S. Markus. 2010. "The Clinical Importance of White Matter Hyperintensities on Brain Magnetic Resonance Imaging: Systematic Review and Meta-Analysis." *BMJ* 341: c3666.

Deco, G., J. Cruzat, J. Cabral, et al. 2019. "Awakening: Predicting External Stimulation to Force Transitions Between Different Brain States." *Proceedings of the National Academy of Sciences of the United States of America* 116: 18088–18097.

Deco, G., V. K. Jirsa, and A. R. McIntosh. 2011. "Emerging Concepts for the Dynamical Organization of Resting-State Activity in the Brain." *Nature Reviews. Neuroscience* 12: 43–56.

Deco, G., M. L. Kringelbach, V. K. Jirsa, and P. Ritter. 2017. "The Dynamics of Resting Fluctuations in the Brain: Metastability and Its Dynamical Cortical Core." *Scientific Reports* 7: 3095.

Demirtaş, M., C. Falcon, A. Tucholka, J. D. Gispert, J. L. Molinuevo, and G. Deco. 2017. "A Whole-Brain Computational Modeling Approach to Explain the Alterations in Resting-State Functional Connectivity During Progression of Alzheimer's Disease." *Neuroimage Clinical* 16: 343–354.

Esteban, O., C. J. Markiewicz, R. W. Blair, et al. 2019. "fMRIPrep: A Robust Preprocessing Pipeline for Functional MRI." *Nature Methods* 16: 111–116.

Fazekas, F., J. B. Chawluk, A. Alavi, H. I. Hurtig, and R. A. Zimmerman. 1987. "MR Signal Abnormalities at 1.5 T in Alzheimer's Dementia and Normal Aging." *American Journal of Roentgenology* 149: 351–356.

Garnier-Crussard, A., F. Cotton, P. Krolak-Salmon, and G. Chételat. 2023. "White Matter Hyperintensities in Alzheimer's Disease: Beyond Vascular Contribution." *Alzheimer's & Dementia* 19: 3738–3748.

Gibbons, L. E., A. C. Carle, R. S. Mackin, et al. 2012. "A Composite Score for Executive Functioning, Validated in Alzheimer's Disease Neuroimaging Initiative (ADNI) Participants With Baseline Mild Cognitive Impairment." *Brain Imaging and Behavior* 6: 517–527.

Girouard, H., and C. Iadecola. 2006. "Neurovascular Coupling in the Normal Brain and in Hypertension, Stroke, and Alzheimer Disease." *Journal of Applied Physiology* 100: 328–335.

Griffis, J. C., N. V. Metcalf, M. Corbetta, and G. L. Shulman. 2021. "Lesion Quantification Toolkit: A MATLAB Software Tool for Estimating Grey Matter Damage and White Matter Disconnections in Patients With Focal Brain Lesions." *NeuroImage: Clinical* 30: 102639.

Idesis, S., C. Favaretto, N. V. Metcalf, et al. 2022. "Inferring the Dynamical Effects of Stroke Lesions Through Whole-Brain Modeling." *NeuroImage: Clinical* 36: 103233.

Jenkins, L. M., A. Kogan, M. Malinab, et al. 2021. "Blood Pressure, Executive Function, and Network Connectivity in Middle-Aged Adults at Risk of Dementia in Late Life." *Proceedings of the National Academy of Sciences of the United States of America* 118: e2024265118.

Kantarovich, K., L. Mwilambwe-Tshilobo, S. Fernández-Cabello, et al. 2022. "White Matter Lesion Load Is Associated With Lower Within- and Greater Between-Network Connectivity Across Older Age." *Neurobiology of Aging* 112: 170–180.

Kobeleva, X., G. Varoquaux, A. Dagher, M. H. Adhikari, C. Grefkes, and M. Gilson. 2022. "Advancing Brain Network Models to Reconcile Functional Neuroimaging and Clinical Research." *NeuroImage: Clinical* 36: 103262.

Li, H., G. Jiang, J. Zhang, et al. 2018. "Fully Convolutional Network Ensembles for White Matter Hyperintensities Segmentation in MR Images." *NeuroImage* 183: 650–665.

Logothetis, N. K. 2003. "The Underpinnings of the BOLD Functional Magnetic Resonance Imaging Signal." *Journal of Neuroscience* 23: 3963–3971.

Logothetis, N. K., and B. A. Wandell. 2004. "Interpreting the BOLD Signal." *Annual Review of Physiology* 66: 735–769.

Maillard, P., E. Fletcher, D. Harvey, et al. 2011. "White Matter Hyperintensity Penumbra." *Stroke* 42: 1917–1922.

Maniega, S. M., M. C. Valdés Hernández, J. D. Clayden, et al. 2015. "White Matter Hyperintensities and Normal-Appearing White Matter Integrity in the Aging Brain." *Neurobiology of Aging* 36: 909–918.

Marques, P., P. Moreira, R. Magalhães, et al. 2016. "The Functional Connectome of Cognitive Reserve." *Human Brain Mapping* 37: 3310–3322.

Min, Z., H. R. Shan, L. Xu, et al. 2021. "Diffusion Tensor Imaging Revealed Different Pathological Processes of White Matter Hyperintensities." *BMC Neurology* 21: 128.

Nagendran, T., R. S. Larsen, R. L. Bigler, et al. 2017. "Distal Axotomy Enhances Retrograde Presynaptic Excitability Onto Injured Pyramidal Neurons via Trans-Synaptic Signaling." *Nature Communications* 8: 625.

Naud, R., and A. Longtin. 2019. "Linking Demyelination to Compound Action Potential Dispersion With a Spike-Diffuse-Spike Approach." *Journal of Mathematical Neuroscience* 9: 3.

Patow, G., L. Stefanovski, P. Ritter, G. Deco, X. Kobeleva, and for the Alzheimer's Disease Neuroimaging Initiative. 2023. "Whole-Brain Modeling of the Differential Influences of Amyloid-Beta and Tau in Alzheimer's Disease." *Alzheimer's Research & Therapy* 15: 210.

Quandt, F., F. Fischer, J. Schröder, et al. 2020. "Higher White Matter Hyperintensity Lesion Load Is Associated With Reduced Long-Range Functional Connectivity." *Brain Communications* 2: fcaa111.

Sanz Perl, Y., S. Fittipaldi, C. Gonzalez Campo, et al. 2023. "Model-Based Whole-Brain Perturbational Landscape of Neurodegenerative Diseases." *eLife* 12: e83970.

Schlemm, E., B. M. Frey, C. Mayer, et al. 2022. "Equalization of Brain State Occupancy Accompanies Cognitive Impairment in Cerebral Small Vessel Disease." *Biological Psychiatry* 92: 592–602.

Schulz, M., C. Malherbe, B. Cheng, G. Thomalla, and E. Schlemm. 2021. "Functional Connectivity Changes in Cerebral Small Vessel Disease—A Systematic Review of the Resting-State MRI Literature." *BMC Medicine* 19: 103.

Shaw, L. M., H. Vanderstichele, M. Knapik-Czajka, et al. 2009. "Cerebrospinal Fluid Biomarker Signature in Alzheimer's Disease Neuroimaging Initiative Subjects." *Annals of Neurology* 65: 403–413.

Škoch, A., B. Rehák Bučková, J. Mareš, et al. 2022. "Human Brain Structural Connectivity Matrices–Ready for Modelling." *Scientific Data* 9: 486.

Sporns, O. 2013. "Structure and Function of Complex Brain Networks." *Dialogues in Clinical Neuroscience* 15: 247–262.

Stern, Y. 2009. "Cognitive Reserve." *Neuropsychologia* 47: 2015–2028.

Suárez, L. E., R. D. Markello, R. F. Betzel, and B. Misic. 2020. "Linking Structure and Function in Macroscale Brain Networks." *Trends in Cognitive Sciences* 24: 302–315.

Svärd, D., M. Nilsson, B. Lampinen, et al. 2017. "The Effect of White Matter Hyperintensities on Statistical Analysis of Diffusion Tensor Imaging in Cognitively Healthy Elderly and Prodromal Alzheimer's Disease." *PLoS One* 12: e0185239.

ter Telgte, A., E. M. C. van Leijsen, K. Wiegertjes, C. J. M. Klijn, A. M. Tuladhar, and F. E. de Leeuw. 2018. "Cerebral Small Vessel Disease: From a Focal to a Global Perspective." *Nature Reviews. Neurology* 14: 387–398.

Thiebaut de Schotten, M., C. Foulon, and P. Nachev. 2020. "Brain Disconnections Link Structural Connectivity With Function and Behaviour." *Nature Communications* 11: 5094.

Tzourio-Mazoyer, N., B. Landeau, D. Papathanassiou, et al. 2002. "Automated Anatomical Labeling of Activations in SPM Using a Macroscopic Anatomical Parcellation of the MNI MRI Single-Subject Brain." *NeuroImage* 15: 273–289.

Vergoossen, L. W. M., J. F. A. Jansen, T. T. van Sloten, et al. 2021. "Interplay of White Matter Hyperintensities, Cerebral Networks, and Cognitive Function in an Adult Population: Diffusion-Tensor Imaging in the Maastricht Study." *Radiology* 298: 384–392.

Wardlaw, J. M., M. C. Valdés Hernández, and S. Muñoz Maniega. 2015. "What Are White Matter Hyperintensities Made of?" *Journal of the American Heart Association* 4: 1–19.

Yang, D., J. Li, Z. Ke, et al. 2023. "Subsystem Mechanisms of Default Mode Network Underlying White Matter Hyperintensity-Related Cognitive Impairment." *Human Brain Mapping* 44: 2365–2379.

Supporting Information

Additional supporting information can be found online in the Supporting Information section.